THE JOURNAL OF BIOLOGICAL CHEMISTRY VOL. 285, NO. 1, pp. 43–53, January 1, 2010

Roscovitine Binds to Novel L-channel ($Ca_V1.2$) Sites That Separately Affect Activation and Inactivation*

Received for publication, October 15, 2009 Published, JBC Papers in Press, November 2, 2009, DOI 10.1074/jbc.M109.076448

Viktor Yarotskyy[‡1], Guofeng Gao[§1], Lei Du[§], Sindura B. Ganapathi[¶], Blaise Z. Peterson[§], and Keith S. Elmslie[‡¶2]

From the Departments of [‡]Anesthesiology, [§]Cellular and Molecular Physiology, and [¶]Pharmacology, Penn State College of Medicine, Penn State University, Hershey, Pennsylvania 17033

L-type ($Ca_V1.2$) calcium channel antagonists play an important role in the treatment of cardiovascular disease. (*R*)-Roscovitine, a trisubstituted purine, has been shown to inhibit L-currents by slowing activation and enhancing inactivation. This study utilized molecular and pharmacological approaches to determine whether these effects result from (*R*)-roscovitine binding to a single site. Using the *S* enantiomer, we find that (*S*)-roscovitine enhances inactivation without affecting activation, which suggests multiple sites. This was further supported in studies using chimeric channels comprised of N- and L-channel domains. Those chimeras containing L-channel domains I and IV showed (*R*)-roscovitine-induced slowed activation like that of wild type L-channels, whereas chimeric channels containing L-channel domain I responded to (*R*)-roscovitine with enhanced inactivation. We conclude that (*R*)-roscovitine binds to distinct sites on L-type channels to slow activation and enhance inactivation. These sites appear to be unique from other calcium channel antagonist sites that reside within domains III and IV and are thus novel sites that could be exploited for future drug development. Trisubstituted purines could become a new class of drugs for the treatment of diseases related to hyperfunction of L-type channels, such as Torsades de Pointes.

Cardiac L-type ($Ca_V1.2$) channels are central to the regulation of a number of physiological processes (1, 2). Activation of these channels in cardiac and smooth muscle generates the calcium influx that triggers calcium release from the sarcoplasmic reticulum (3) to induce contraction. In contrast, inactivation of these channels provides a negative feedback mechanism to limit calcium influx into the cardiac myocyte, which helps protect from excessive calcium influx that can lead to cardiac arrhythmias (3). L-channel antagonists are routinely used to treat cardiovascular diseases, such as hypertension and angina pectoris (4–8). Therefore, drugs that inhibit L-channel function have high clinical relevance.

Roscovitine is a 2,6,9-trisubstituted purine that was originally developed as a selective blocker of cyclin-dependent kinases (9) and is currently undergoing phase II clinical trials as an anticancer drug (10). It has recently become apparent that roscovitine can affect voltage-dependent ion channels at clinically relevant concentrations (10–50 μM) (10–13). We (14, 15) and others (16, 17) have shown that (*R*)-roscovitine differentially affects voltage-dependent calcium channels. (*R*)-Roscovitine has two effects on Ca_V2 channels (N-type, P/Q-type, and R-type), which are a rapid onset agonist effect and a more slowly developing antagonist effect (14, 15). The agonist effect results from (*R*)-roscovitine specifically binding to activated Ca_V2 channels to slow channel closing (14, 15), which results in a significant enhancement of action potential induced calcium influx (14). The antagonist effect appears to result from (*R*)-roscovitine preferentially enhancing occupancy of a "resting" inactivated state to inhibit channel activity (18). Interestingly, the racemic variant (*S*)-roscovitine has been found to exhibit only an antagonist effect on N-channels, which is one result supporting unique binding sites for the agonist *versus* antagonist effects (14, 15, 18).

L-type channels are also inhibited by (*R*)-roscovitine, but by a unique mechanism relative to N-channels (19). L-channel inhibition results from slowed activation and enhanced open state voltage-dependent inactivation (VDI),[3] but the resting inactivated state is not affected. These two effects were characterized by approximately equal EC_{50} values (~30 μM), which suggested a single binding site. However, the Hill coefficient for (*R*)-roscovitine-induced slowed activation was ~1, whereas that for enhanced inactivation was >2, which could result from multiple binding sites (19). Intracellularly applied (*R*)-roscovitine failed to affect L-channel activity, which supported an extracellularly exposed binding site(s) mediating both effects. The differential effect of (*R*)-roscovitine on N-type *versus* L-type channels provides an opportunity to localize the L-channel binding site(s) by making chimeric channels. In addition, the differential effect of racemic roscovitine variants on N-channels led us to investigate if the L-channel site(s) also showed chiral specificity.

We found that (*S*)-roscovitine enhanced L-channel VDI without slowing activation, which supports separate binding sites for these effects. In addition, the chimeric channels showed that the L-channel domain I (L-DI) is both necessary

* This work was supported, in whole or in part, by National Institutes of Health Grant HL074143 (to B. Z. P.). This work was also supported in part by American Heart Association Predoctoral Fellowship 0715336U (to S. B. G.), startup funds from the Department of Anesthesiology at the Penn State College of Medicine (to K. S. E.), and grants from the Pennsylvania Department of Health using Tobacco Settlement Funds (to K. S. E. and B. Z. P.).

[1] Both of these authors contributed equally to this work.

[2] To whom correspondence should be addressed: Dept. of Anesthesiology H187, Penn State College of Medicine, 500 University Dr., Hershey, PA 17033.

[3] The abbreviations used are: VDI, voltage-dependent inactivation; HSD, honestly significant difference; L-DI, L-DII, L-DIII, and L-DIV, L-channel domains I, II, III, and IV, respectively; N-DI, N-DII, N-DIII, and N-DIV, N-channel domains I, II, III, and IV, respectively; WT, wild type; RR_{SA}, roscovitine receptor site mediating slowed activation; RR_{EI}, roscovitine receptor site mediating enhanced inactivation.

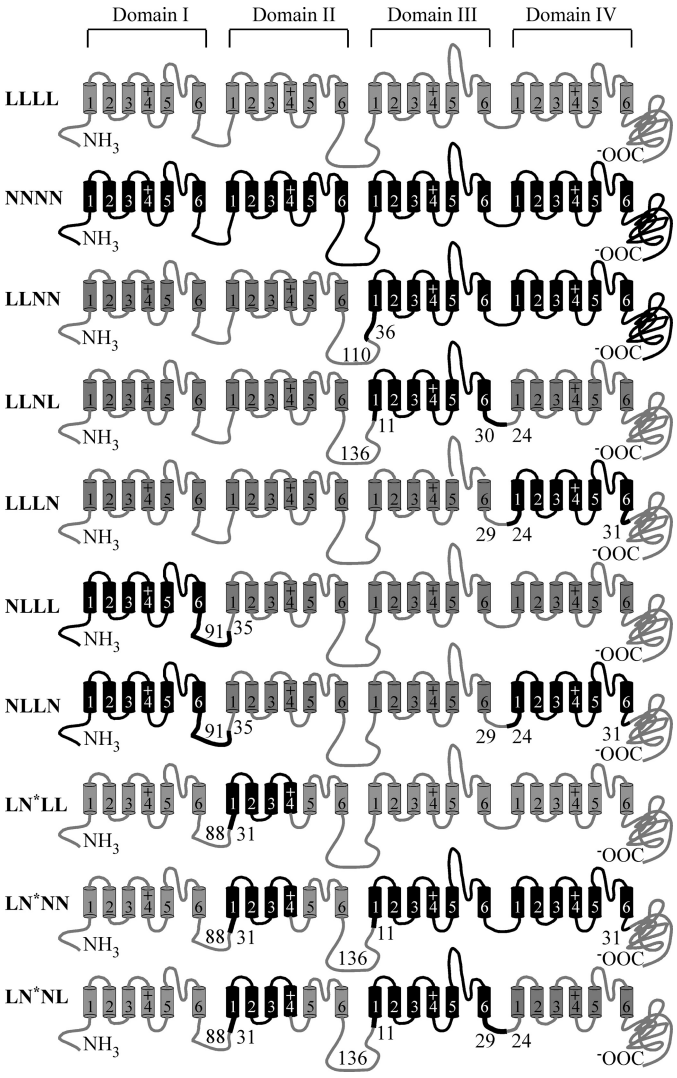

FIGURE 1. **The calcium channel constructs used in this study.** Domains I–IV are shown with each domain represented as a set of six transmembrane segments, *1–6*. Loops between the segments and domains are shown as *lines*. N-channel structures are shown in *black*, whereas those from the L-channel are in *gray*. The *numbers* at the connections between N-type and L-type domains show the number of amino acid residues within that intracellular loop contributed by a given channel type. To highlight the connection, the N-channel section is shown as a *thicker line*. For LN*LL, LN*NN, and LN*NL chimeras, *N** refers to an engineered N-DII, which is composed of N-type transmembrane segments 1–4 and L-type transmembrane segments 5 and 6. The loop between segments 4 and 5 is from the L-channel.

and sufficient for the (*R*)-roscovitine-induced enhancement of VDI, but slowed activation requires both L-DI and L-DIV. These results reveal novel sites on the L-type calcium channel that can be exploited for the development of drugs that can specifically target the activation or inactivation function.

EXPERIMENTAL PROCEDURES

Construction of Chimeric Channels—Chimeric calcium channels (Fig. 1) were constructed using cDNAs encoding the rabbit cardiac L-channel (GenBank™ number X15539) and rat neuronal N-channel (GenBank™ number AF055477; generously provided by Dr. Lucie Parent) α1 subunits. Briefly, N-channel domains were amplified by PCR, subcloned into pCR-Blunt II-TOPO vectors (Invitrogen), excised by restriction enzyme digestion, and subcloned in frame into an engineered L-channel. The sequences of the wild type (WT) and mutant channels were aligned using Vector NTI (Invitrogen), and domain boundaries were placed in regions of high amino acid sequence homology. The engineered L-channel was generated by introducing unique AgeI and NotI sites into the intracellular linkers between the II/III (nucleotide 2751) and III/IV (nucleotide 3680) domains, respectively, using silent mutagenesis via the QuikChange II site-directed mutagenesis kit (Stratagene, La Jolla, CA). A unique XbaI site was introduced at nucleotide 4633 in the C terminus of the engineered channel using a similar strategy. The overall integrity of the engineered L-channel and each chimera was confirmed by qualitative restriction enzyme digests, DNA sequence analyses, Western blot analysis, and patch clamp electrophysiology .

The chimeric channels were constructed as described below. For NNLL, L-DI and L-DII (Met^{1}–Asn^{917}) were replaced by N-DI and N-DII (Met^{1}–Asn^{1134}). N-DI and N-DII were amplified from full-length $Ca_V2.2$ and subcloned into the HindIII/AgeI sites of the engineered L-channel. For LLNN, L-DIII and L-DIV (Leu^{895}–Leu^{2171}) were replaced by N-DIII and N-DIV (Asp^{1112}–Cys^{2333}). The construction of this chimera did not utilize the engineered L-channel containing the introduced AgeI and NotI sites. Instead, a XbaI site at nucleotide 2678 was introduced into the L-channel, resulting in a missense mutation of a glutamate to arginine at position 894. For NLLL, L-DI (Met^{1}–Cys^{519}) was replaced by N-DI (Met^{1}–Pro^{447}). The insert for this chimera was constructed via overlap extension PCR. Briefly, N-DI and L-DII were amplified from full-length $Ca_V2.2$ and $Ca_V1.2$, respectively. The PCR products of these two domains contain a small region of overlap. They were then combined and used as templates in a second round of PCR. The final PCR product was subcloned into the HindIII/AgeI sites of the engineered L-channel. For LNLL, L-DII (Ala^{524}–Val^{781}) was replaced by N-DII (Ser^{452}–Val^{909}). This chimera was constructed using a strategy similar to that described for NLLL above. For LLNL, N-DIII (Arg^{1137}–Ala^{1443}) was amplified from full-length $Ca_V2.2$ and ligated into the AgeI/NotI sites of the engineered L-channel, thereby replacing L-DIII (Arg^{920}–Ala^{1226}). For LLLN, N-DIV (Pro^{1445}–Ile^{1741}) was amplified from full-length $Ca_V2.2$ and ligated into the NotI/BstEII sites of the engineered L-channel, thereby replacing L-DIV (Pro^{1228}–Ile^{1542}). For LNNL, N-DII and N-DIII were amplified from $Ca_V2.2$ with a 5′ primer containing an AscI site and a 3′ primer containing a NotI site, excised with AscI/NotI, and subcloned into the AscI/Not sites of LLNL. For LNNN, N-DIV was excised with NotI/XbaI from LLLN and subcloned into the NotI/XbaI sites of LNNL. For NNNL, N-DI was excised with HindIII/AscI from NLLL and subcloned into the HindIII/AscI sites of LNNL. For NNLN, N-DIV was excised with NotI/XbaI from LLLN and subcloned into the NotI/XbaI sites of NNLL. For NLLN, N-DI was excised with HindIII/AscI from NLLL and subcloned into the HindIII/AscI sites of LLLN. For L(l/n)LL, L-DII transmembrane segments 1–4 were amplified with a 5′ primer containing an AscI site and a 3′ primer (5′-ACC AGG TTC CTC AGG GAG TTC CAG TAC CTT GTA ATT TTG-3′) using NLLL as template, and N-DII transmembrane segments 5 and 6 with N-type intracellular linker between transmembrane segments 4

and 5 were amplified with a 5′ primer (5′-ATT ACA AGG TAC TGG AAC TCC CTG AGG AAC CTG GTT G-3′) and a 3′ primer lying downstream of an existing BfrI site in the WT α_{1C} plasmid (pCDNA3). The final overlap PCR products were amplified using the above 5′ primer containing an AscI site and the above 3′ primer lying downstream of an existing BfrI site. The resulting PCR products were excised with AscI/BfrI and subcloned into the AscI/BfrI sites of LNLL to make L(l/n)LL. For LN*LL (also known as L(n/l)LL), N-DII transmembrane segments 1–4 were amplified with a 5′ primer containing an AscI site and a 3′ primer (5′-CAG GTT GCT CAA GGA GTT CCA ATA CTT GGT GAC TTT GAA AAT CCT CAG-3′) using LNLL as template, and L-DII transmembrane segments 5 and 6 with an L-type intracellular linker between transmembrane segments 4 and 5 were amplified with a 5′ primer (5′-GTC ACC AAG TAT TGG AAC TCC TTG AGC AAC CTG GTG GCC-3′) and a 3′ primer lying downstream of an existing BfrI site in WT α_{1C} plasmid (pCDNA3). The final overlap PCR products were amplified using the above 5′ primer containing an AscI site and the above 3′ primer lying downstream of an existing BfrI site. The resulting PCR products were excised with AscI/BfrI and subcloned into the AscI/BfrI sites of LNLL to make L(n/l)LL. For LN*NN (also known as L(n/l)NN), first L-DIV in LLNL was replaced by N-DIV from LLLN to make a different LLNN maintaining the engineered unique AgeI site between the II and III domains, NotI sites between the III and IV domains, and XbaI site just after domain IV. Then the chimera domain II n/l was excised with AscI/BfrI from L(n/l)LL and subcloned into the AscI/BfrI sites of LLNN to make L(n/l)NN. For LN*NL (also known as L(n/l)NL), the fragment containing the chimera domain II n/l and N-DIII was excised with AscI/NotI from L(n/l)NN and ligated into the AscI/NotI sites of LNNL to make L(n/l)NL. The mutation and integrity of the mutant cDNAs was confirmed by qualitative restriction map analysis and directional DNA sequence analysis of the entire subcloned region. Functional expression of the mutant cDNAs was confirmed by Western blot analysis and patch clamp electrophysiology.

HEK Cell Transfection—We utilized either the calcium phosphate precipitation method (19) or Lipofectamine 2000 (following the manufacturer's directions) to transfect HEK 293 cells with WT L-, N-, and chimeric channels, which provided highly reproducible expression 24–72 h after transfection. HEK293 cells were maintained in standard Dulbecco's modified Eagle's medium containing 10% fetal bovine serum and 1% antibiotic-antimycotic mixtures (regular medium) at 37 °C in a 5% CO_2 incubator. HEK293 cells were transfected with cDNA plasmids using the following molar ratio: 1 α_1 subunit (L-, N-, or chimeric channel):1 $\alpha_2\delta$:1 β_{1b}:1 TAG (to increase expression efficiency):0.2 green fluorescent protein (to visualize transfected cells). The transfected cells were split next day into 35-mm dishes that served as the recording chamber.

Measurement of Ionic Currents—Cells were voltage-clamped using the whole-cell configuration of the patch clamp technique. Pipettes were pulled from Schott 8250 glass (Garner Glass, Claremont, CA) on a Sutter P-97 puller (Sutter Instruments Co., Novato, CA). Currents were recorded using an Axopatch 200A amplifier (Molecular Devices, Sunnyvale, CA) and digitized with the ITC-18 data acquisition interface (Instrutech Corp., Port Washington, NY). Experiments were controlled by a Power Macintosh G3 computer (Apple Computer, Cupertino, CA) running S5 data acquisition software written by Dr. Stephen Ikeda (NIAAA, National Institutes of Health, Bethesda, MD). Leak current was subtracted online using a P/4 protocol. All recordings were carried out at room temperature, and the holding potential was −120 mV. Whole-cell currents were digitized depending on test step duration at 50 (25 ms), 10 (200 ms), and 4 (1000 ms) kHz after analog filtering at 1–10 kHz.

Data Analysis—Data were analyzed using IgorPro (WaveMetrics, Lake Oswego, OR) running on a Macintosh computer. Step currents were measured as the average of 1 ms at the end of the voltage step. Activation τ (τ_{Act}) was determined by fitting a single exponential function to the step current after a 0.3-ms delay (15). Inactivation τ (τ_{Inact}) was determined by fitting a single exponential function from peak step current to the end of the step. The effect of roscovitine on inactivation of L-type or chimeric calcium channels was measured by using either 200- or 1000-ms voltage steps. The magnitude of inactivation was measured from either the I_{End}/I_{Peak} ratio, where I_{End} was measured at the end of the step and I_{Peak} was peak current, or as the I_{Post}/I_{Pre} ratio from a triple pulse protocol consisting of identical 25-ms pre- and postpulse steps (to elicit peak current) bracketing a 200-ms test pulse to voltages ranging from −120 to +80 mV. Group data were calculated as mean ± S.D. throughout the paper. A paired *t* test was used for within-cell comparisons. One-way analysis of variance with Tukey's HSD *post hoc* test was used to test for differences among three or more independent groups.

Solutions—The internal pipette solution contained 104 mM NMG-Cl, 14 mM creatine-PO_4, 6 mM $MgCl_2$, 10 mM NMG-HEPES, 5 mM Tris-ATP, 0.3 mM Tris-GTP, and 10 mM NMG-EGTA with osmolarity of 280 mosM and pH 7.3. The external recording solution contained 30 mM $BaCl_2$, 100 mM NMG-Cl, 10 mM NMG-HEPES, osmolarity of 300 mosM, and pH 7.3. We used Ba^{2+} as the permeant ion to exclude Ca^{2+}-dependent inactivation (25, 26), since we have previously demonstrated that (*R*)-roscovitine enhances VDI but does not affect calcium-dependent inactivation (19). Both (*R*)- and (*S*)-roscovitine were prepared as a 50 mM stock solution in DMSO and stored at −30 °C. All external solutions contained the same DMSO concentration so that the roscovitine concentration was the sole variable when changing solutions. Test solutions were applied from a gravity-fed perfusion system with an exchange time of 1–2 s.

Chemicals—All experiments utilized (*R*)-roscovitine from LC Laboratories (Woburn, MA) and (*S*)-roscovitine from Alexis Biochemicals (San Diego, CA). Dulbecco's modified Eagle's medium/F-12, Dulbecco's modified Eagle's medium, fetal bovine serum, 100× antibiotic/antimycotic, and Lipofectamine 2000 were from Invitrogen. Other chemicals were obtained from Sigma.

RESULTS

(S)-Roscovitine Does Not Affect L-channel Activation—We have shown that (*R*)-roscovitine significantly slows activation and enhances inactivation of L-type channels and hypothesized

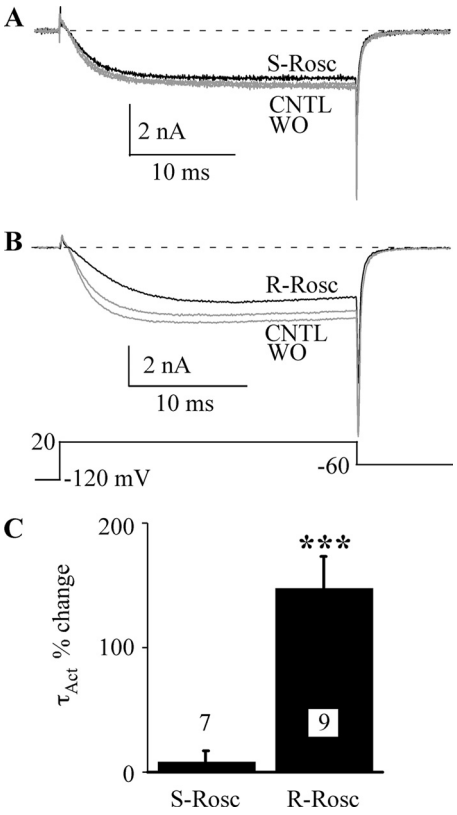

FIGURE 2. **(*S*)-Roscovitine does not slow activation of L-type channels.** *A*, L-current was activated during 25-ms voltage steps to +20 mV. 100 μM (*S*)-roscovitine (*S-Rosc*, *black*) slightly decreased current but did not alter activation relative to control (*CNTL*, gray) and washout (*WO*, *gray*). *B*, in the same cell, 100 μM (*R*)-roscovitine (*R-Rosc*, *black*) slowed L-current activation. *C*, the percentage change in τ_{Act} at +20 mV induced by application of 100 μM (*R*)-roscovitine was significantly different (***, $p < 0.001$) from zero, whereas that for (*S*)-roscovitine was not. The data are shown as mean ± S.D., and the number of cells examined is indicated.

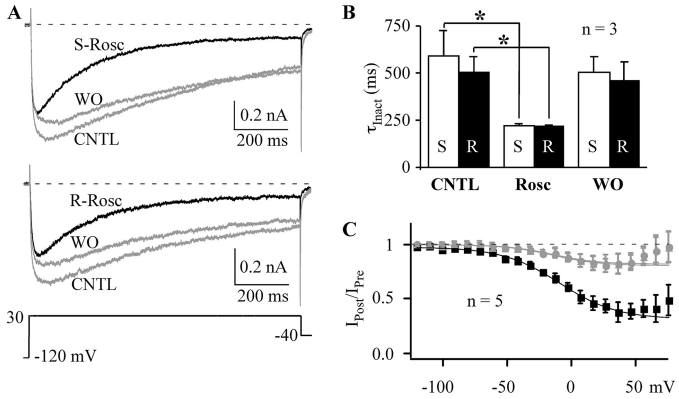

FIGURE 3. **(*S*)-Roscovitine enhances inactivation of L-type channels.** *A*, L-currents were evoked by 1-s voltage steps to +30 mV to examine the effect of either 100 μM (*S*)-roscovitine (*top*; *S-Rosc*) or (*R*)-roscovitine (*bottom*; *R-Rosc*) compared with control and washout (*CNTL* and *WO*, *gray*). *B*, τ_{Inact} at +30 mV is significantly decreased by application of either 100 μM (*S*)-roscovitine (*S*) or (*R*)-roscovitine (*R*) compared with control (*, $p < 0.05$). *C*, (*S*)-roscovitine enhanced VDI. L-currents were evoked by a three-pulse protocol comprised of two 25-ms steps to +30 mV (*Pre* and *Post*) flanking a 200-ms inactivating pulse (−120 to +80 mV). The voltage dependence of inactivation is shown as the I_{Post}/I_{Pre} ratio *versus* inactivation voltage, where I_{Post} and I_{Pre} represent the current measured at the end of the pre- and postpulses, respectively. Control (*gray circle*), 100 μM (*S*)-roscovitine (*black square*), and washout (*gray triangle*) data from −120 to 50 mV (peak inactivation) were fitted by Boltzmann functions to yield $V_{½} = -14.7$, −9.41, and −14.4 mV, slope factor = −18.5, −22.2, −17.5, and maximum inactivation = 0.19, 0.66, and 0.18, for control, (*S*)-roscovitine, and washout, respectively.

that a single extracellular binding site mediated both effects (19). We further investigated this idea by examining the effect of (*S*)-roscovitine on L-type channels, which was useful in differentiating multiple roscovitine binding sites on N-type channels (15, 17, 18). Using 25-ms voltage steps to +20 mV, we verified that 100 μM (*R*)-roscovitine slowed L-channel activation (15, 19) (Fig. 2). However, the activation rate was not altered by the application of 100 μM (*S*)-roscovitine (Fig. 2*A*), which was estimated by fitting the +20 mV step current using a single exponential function to generate τ_{Act}. The average change in τ_{Act} induced by (*S*)-roscovitine was 8.6 ± 8.5% (±S.D., $n = 7$), whereas the (*R*)-roscovitine-induced increase of τ_{Act} was 148.6 ± 24.8% ($n = 9$, $p < 0.001$; Fig. 2*C*). Thus, the L-channel binding site involved with slowed activation shows stereo-selectivity for roscovitine.

(S)-Roscovitine Enhances L-channel VDI—The inability of (*S*)-roscovitine to slow L-channel activation could be explained by low affinity of a single roscovitine binding site for the *S* enantiomer. If this were true, inactivation should also be insensitive to (*S*)-roscovitine. This hypothesis was tested using 1000-ms voltage steps to +30 mV to measure VDI (30 mM Ba^{2+}). Fig. 3 shows typical L-current traces recorded from the same cell exposed to either 100 μM (*S*)- or (*R*)-roscovitine. The speed of inactivation (τ_{Inact}) was determined from single exponential fits to the inactivating portion of the current (peak to end). Counter to our hypothesis, (*S*)-roscovitine increased inactivation to a degree similar to that of (*R*)-roscovitine (Fig. 3). (*S*)-Roscovitine decreased τ_{Inact} from 591 ± 133 to 220 ± 11 ms ($p < 0.05$, $n = 3$), whereas τ_{Inact} was decreased from 504 ± 84 to 216 ± 7 ms ($p < 0.05$, $n = 3$) by (*R*)-roscovitine (Fig. 3*B*). There was no significant difference in τ_{Inact} between (*S*)-roscovitine and (*R*)-roscovitine. The L-channel binding site that mediates roscovitine-induced enhancement of inactivation does not show stereo-selectivity.

The effect of (*S*)-roscovitine on the voltage dependence of inactivation was determined using a three-pulse protocol where the ratio of the postpulse/prepulse (25 ms, +30 mV) current (I_{Post}/I_{Pre}) was used to monitor inactivation induced by 200-ms inactivating steps ranging in voltage from −120 to +80 mV. Under control conditions (30 mM Ba^{2+}), the inactivation *versus* voltage relationship was U-shaped (Fig. 3*C*), which was more prominent than we observed previously using 10 mM Ba^{2+} (19). The reason for this difference is unknown, but as we did with our previous data, we fit the inactivation *versus* voltage data from −120 to +50 mV (peak inactivation) using a single Boltzmann equation (Fig. 3*C*). (*S*)-Roscovitine increased the magnitude of inactivation so that the inactivation *versus* voltage relationship became less U-shaped. Maximal inactivation from the Boltzmann fit increased from 0.19 ± 0.01 in control and 0.18 ± 0.02 for recovery to 0.66 ± 0.03 by (*S*)-roscovitine. Boltzmann fitting of the I_{Post}/I_{Pre} *versus* voltage relationship showed a small (~5 mV) (*S*)-roscovitine-induced right shift in half-inactivation voltage ($V_{½}$) and a small (*e*-fold/4 mV) decrease in slope (Fig. 3*C*) that was also observed with (*R*)-roscovitine (see Fig. 6*A*). Maximal inactivation was increased from 0.23 in control to 0.67 in (*R*)-roscovitine, which is very

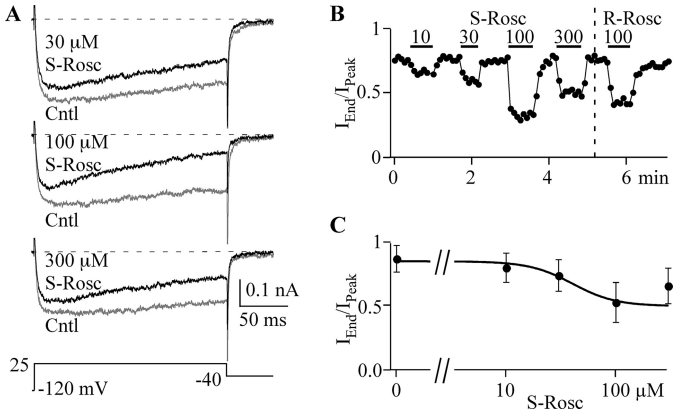

FIGURE 4. **The dose-response relationship for the (*S*)-roscovitine-induced enhancement of inactivation.** *A*, representative traces from a single cell show the enhancement of inactivation induced by application of 30, 100, and 300 μM (*S*)-roscovitine (*dark*) compared with control (*gray*). Currents were evoked by 200-ms steps to 25 mV. *B*, inactivation was quantified as the I_{End}/I_{Peak} ratio, where I_{End} was measured at the end of the 200-ms step (+25 mV) and I_{Peak} was measured at the peak of the step current. The effect on inactivation is shown for 10, 30, 100, and 300 μM (*S*)-roscovitine (*S-rosc*) and 100 μM (*R*)-roscovitine (*R-rosc*). *C*, the dose-response relationship for the effect of (*S*)-roscovitine on inactivation is shown along with a fit (*smooth line*) using the Hill equation with an EC_{50} = 41.1 μM and a Hill coefficient = 4.5. The data are presented as mean ± S.D. of 5–11 cells.

similar to our observations with (*S*)-roscovitine. These results suggest that the L-channel site mediating enhanced inactivation does not differentiate between (*R*)- and (*S*)-roscovitine.

Steep Dose-Response Relationship for (S)-Roscovitine—The dose-response relationship of (*R*)-roscovitine showed similar EC_{50} values for both slowed activation and enhanced inactivation (20–30 μM), which supported a single binding site (19). However, the Hill coefficient was close to 1 (1.2) for slowed activation, whereas that for enhanced inactivation was >2 (2.3), which suggested separate binding sites for these two effects. The differential sensitivity of slowed activation for (*R*)- *versus* (*S*)-roscovitine supports the latter idea. We further investigated the enhanced inactivation by determining the EC_{50} for (*S*)-roscovitine. Inactivation was measured as the I_{End}/I_{Peak} ratio calculated from 200-ms steps to +25 mV. (*S*)-Roscovitine increased inactivation in a dose-dependent manner from 10 to 100 μM, but the response to 300 μM was reproducibly reduced relative to that of 100 μM. This effect was also observed in (*R*)-roscovitine (19). The dose-response data were fit (0–100 μM) using the Hill equation to yield EC_{50} = 41.1 ± 0.1 μM and a Hill coefficient of 4.47 ± 0.03 (Fig. 4). Both of these values are larger than that obtained from (*R*)-roscovitine (19). One thing that is clear from these data is that the binding site mediating enhanced inactivation shows a Hill coefficient of >2, suggesting positive cooperativity. One explanation for this cooperativity is that roscovitine selectively binds to inactivated channels to enhance VDI.

Chimeric N-L Channels—We were interested in localizing the L-type channel structures that mediate both roscovitine-induced effects to further investigate the hypothesis of multiple roscovitine binding sites. We focused on a chimeric strategy that had been previously exploited to determine DHP binding sites on L-type channels (20) but needed to establish that the (*R*)-roscovitine effect on L-channels was unique. We had previously demonstrated that (*R*)-roscovitine uniquely affected

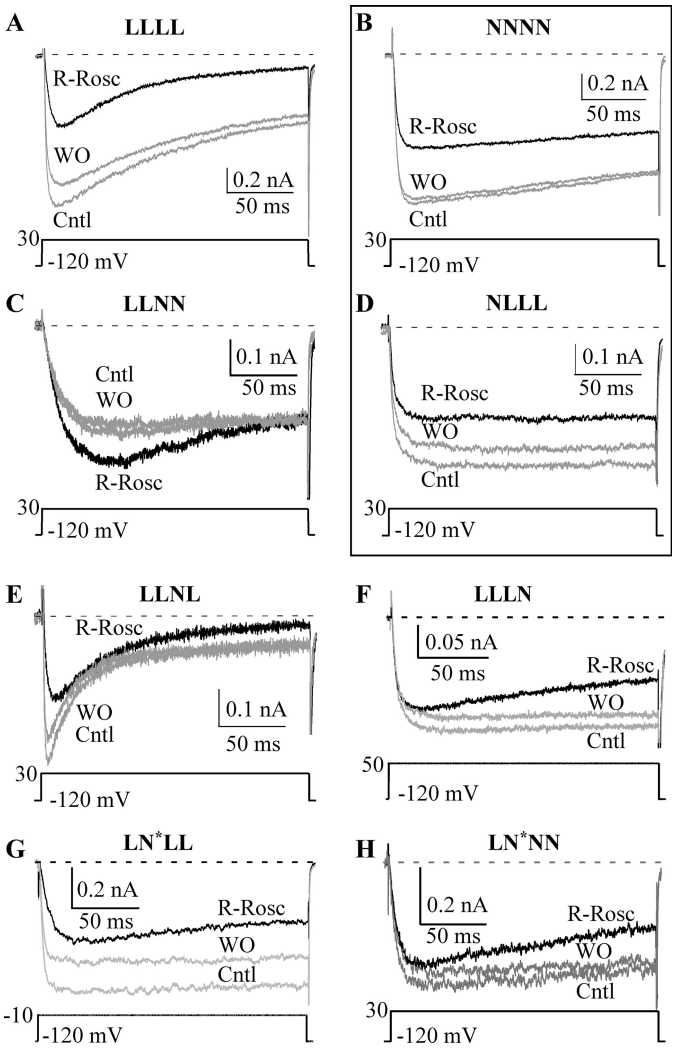

FIGURE 5. **(*R*)-roscovitine enhanced inactivation of channels containing the L-channel domain I.** Currents evoked by 200-ms steps to the indicated voltage for LLLL (*A*), NNNN (*B*), LLNN (*C*), NLLL (*D*), LLNL (*E*), LLLN (*F*), LN*LL (*G*), and LN*NN (*H*) channels were used to evaluate the effect of 100 μM (*R*)-roscovitine (*black traces*). (*R*)-Roscovitine enhanced inactivation of WT L- (LLLL), LLNL, LLLN, LN*LL, and LN*NN channels but failed to alter inactivation of WT N- (NNNN) and NLLL channels.

L-channel activation because N-channel activation was slowed only at voltages of <0 mV and L-channel activation was slowed at all voltages (14, 19). However, our recordings of native N-current (bullfrog sympathetic neurons) showed enhanced inactivation during voltage steps (peak current) (14). Surprisingly, our data from N-type channels expressed in HEK293 cells failed to reproduce those results (Figs. 5 and 6). Inactivation during 200-ms steps to +30 mV was not enhanced (Fig. 5*B*), and the mean I_{Post}/I_{Pre} ratio was not changed at any voltage by 100 μM (*R*)-roscovitine (Fig. 6*B*). Single Boltzmann equation fits from −120 mV to peak inactivation (+10 mV) yielded maximum inactivation of 0.48 ± 0.05 in control *versus* 0.47 ± 0.03 (±S.D., n = 6, not significant) in (*R*)-roscovitine. Thus, (*R*)-roscovitine does not enhance U-type inactivation of N-type calcium channels (21) expressed in HEK293 cells. These results demonstrate that N-L chimeric channels can be used to localize L-channel domain(s) transducing the roscovitine effects.

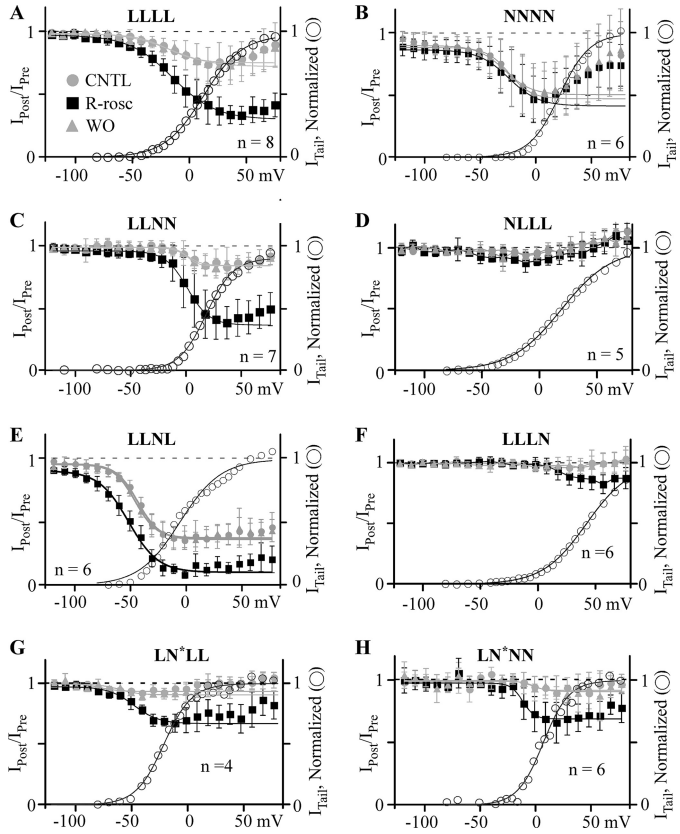

FIGURE 6. **(*R*)-Roscovitine enhances VDI of channels containing L-DI.** Inactivation was measured as the I_{Post}/I_{Pre} ratio using the three-pulse protocol described in the legend to Fig. 3. Control (*CNTL*, *gray circles*), 100 μM (*R*)-roscovitine (*R-Rosc*, *black squares*), and washout (*WO*, *gray triangles*) data from −120 to peak inactivation were fitted using a single Boltzmann equation (*smooth lines*) to yield $V_{1/2}$ and slope as described in the legend to Fig. 3. The activation-voltage relationship in control (*right axis*, *open circles*) is superimposed here for comparison with the voltage dependence of inactivation. The activation-voltage relationship was fitted by a single Boltzmann function (*smooth lines*), and the relationship was normalized to the maximum current from that fit. (*R*)-Roscovitine enhanced VDI of LLLL (*A*), LLNN (*C*), LLNL (*E*), LLLN (*F*), LN*LL (*G*), and LN*NN (*H*) channels but did not affect NNNN (*B*) and NLLL (*D*) channels. For LLLL channels (*A*), the Boltzmann parameters for inactivation were $V_{1/2}$ = −19.6, −15.3, and −16.4; slope = −13.6, −19.1, and −18.7; maximum inactivation = 0.23, 0.67, and 0.27 for control, (*R*)-roscovitine, and washout, respectively, whereas those parameters for activation were $V_{1/2}$ = 15.0 and slope = 15.6. For NNNN channels (*B*), the Boltzmann parameters for inactivation were $V_{1/2}$ = −24.1, −24.7, and −28.6; slope = −13.9, −14.5, and −15.6; maximum inactivation = 0.48, 0.47, and 0.45 for control, (*R*)-roscovitine, and washout, respectively, whereas those for activation were $V_{1/2}$ = 21.0 and slope = 12.6. For LLNN channels (*C*), the Boltzmann parameters for inactivation were $V_{1/2}$ = 1.4, 0.8, and 0.6 mV; slope = −6.8, −10.0, and −5.0; maximum inactivation = 0.15, 0.6, and 0.15 for control, (*R*)-roscovitine, and washout, respectively, whereas those parameters for activation were $V_{1/2}$ = −17.7 mV and slope = 9.6. It was not possible to accurately describe the inactivation data from the NLLL chimera (*D*) using the Boltzmann equation, but for activation, the Boltzmann parameters were $V_{1/2}$ = 18.7 and slope = 21.7. For LLNL channels (*E*), the Boltzmann parameters for inactivation were $V_{1/2}$ = −43.5, −51.8, and −45.8 mV; slope = −9.8, −13.3, and −9.5; maximum inactivation = 0.6, 0.81, and 0.58 for control, (*R*)-roscovitine, and washout, respectively, whereas those for activation were $V_{1/2}$ = −9.2 mV and slope = 18.1. For LLLN channels (*F*), inactivation in control was too small to allow for Boltzmann fitting. However, the Boltzmann parameters for activation were $V_{1/2}$ = 41.7 mV and slope = 19. For LN*LL channels (*G*), the Boltzmann parameters for inactivation were $V_{1/2}$ = −79.1, −48.5, and −60.8 mV; slope = −9.1, −11.2, and −9.0; maximum inactivation = 0.07, 0.30, and 0.09 for control, (*R*)-roscovitine, and washout, respectively, whereas those parameters for activation were $V_{1/2}$ = −21.7 mV and slope = 12.5. For LN*NN channels (*H*), the Boltzmann parameters for inactivation were $V_{1/2}$ = −2.4, −12.1, and −2.5 mV; slope = −4.9, −5.2, and −7.1; maximum inactivation = 0.07, 0.29, and 0.09 for control, (*R*)-roscovitine, and washout, respectively, whereas those parameters for activation were $V_{1/2}$ = 6.5 mV and slope = 11.6.

Initially, chimeric channels were generated by placing one or two N-channel domains into an L-channel backbone. Accordingly each domain is identified by a single-letter code corresponding to the contributing channel type (L for L-type and N for N-type). For example, the WT L-channel is LLLL, whereas the chimera with domain III of the N-type channel in the L-channel backbone is indicated by LLNL. The data were gathered from five L-channel-based chimeric channels (LLNN, NLLN, NLLL, LLNL, and LLLN) as well as the two WT channels (LLLL and NNNN). However, two other chimeras (NNLL and LNLL) failed to generate measurable current. Additional chimeras were generated by inserting a single L-channel domain into the N-channel backbone (*e.g.* LNNN, NNLN, and NNNL), but none of these generated measurable current. Our detailed investigation into these non-functional chimeric channels revealed N-DII as the problem. We further investigated this domain using hemidomain chimeras that separated N-DII into a V-region that encompassed transmembrane segments S1–S4 and a P-region with S5 and S6 (see "Experimental Procedures" and Fig. 1), which revealed that chimeric channels containing the N-DII P-region (S5 and S6) failed to generate functional channels (not shown). To overcome this problem, we engineered a domain II with an N-channel V-region (S1–S4) and L-channel P-region (S5 and S6) (see "Experimental Procedures" and Fig. 1), which we call N*. This engineered domain II allowed us to generate functional chimeric channels with a predominately N-type backbone, including LN*NN, and LN*NL.

Inactivation—VDI was examined using the triple pulse protocol described above (Fig. 6). The first chimeric channel tested was LLNN, which would potentially allow us to localize the roscovitine binding sites to half of the channel. 100 μM (*R*)-roscovitine enhanced VDI of the LLNN chimera (Figs. 5*C* and 6*C*) similar to that observed with the WT L-channel (LLLL) (Figs. 5*A* and 6*A*), which suggests that the relevant binding site is within domain I and/or II. This was further supported by (*R*)-roscovitine-enhanced VDI for both the LLNL (Figs. 5*E* and 6*E*) and LLLN (Figs. 5*F* and 6*F*) chimeras. The role of L-DI was examined by applying 100 μM (*R*)-roscovitine to the NLLL chimera, which, like the WT N-channel (NNNN), failed to alter VDI (Figs. 5*D* and 6*D*). If L-DI is the relevant domain, we should be able to transfer enhanced inactivation to the N-channel by introducing replacing N-DI with the L-channel homolog. Unfortunately, the LNNN chimera contained N-DII, which caused our chimeric channels to fail to express current (see above and "Experimental Procedures"). This problem was overcome by introducing the N* domain discussed above. As a first step, we examined the effect of the N* domain on (*R*)-roscovitine-enhanced VDI by generating the LN*LL chimera, which showed enhanced inactivation like the WT L-channel. This result also supports L-DI as the relevant domain because introduction of the N-DII V-region into the L-channel failed to affect (*R*)-roscovitine-enhanced VDI. Placing L-DI into the N-channel to generate the LN*NN chimera made this channel respond to 100 μM (*R*)-roscovitine with enhanced VDI that was significantly different from that of WT N-channel but similar to that of WT L-channels (see Fig. 9*A*).

Our hypothesis is that (*R*)-roscovitine enhances VDI of chimeric channels containing L-DI, but VDI is characterized by a

monotonic increase of inactivation with voltage. Thus, the (*R*)-roscovitine-induced enhancement of inactivation must show such an increase with voltage if VDI is the affected inactivation mechanism. Consistent with this hypothesis, the (*R*)-roscovitine enhancement of inactivation monotonically increased with depolarization for all chimeric channels containing L-DI. This effect was quantified by Boltzmann equation fitting of the inactivation *versus* voltage relationship (−120 to +50 mV), which revealed subtle differences in the responses of LLLL, LLNN, LLNL, LN*LL, and LN*NN channels to (*R*)-roscovitine (Fig. 6). All of the chimeric channels showed a reduction in the steepness of the inactivation *versus* voltage relationship by (*R*)-roscovitine so that the Boltzmann slope factor was typically reduced by *e*-fold/3 mV, but the change in $V_{½}$ was more variable (see the legend to Fig. 6). One problem was that maximal inactivation was small for some chimeric channels under control conditions, which made it difficult to assess the Boltzmann fitting parameters. However, it is clear that VDI is the inactivation mechanism affected by (*R*)-roscovitine.

Statistical comparisons of all of the channels tested are shown in Fig. 9*A*. For this comparison, we measured the enhancement of fractional inactivation induced by (*R*)-roscovitine (Δ*Rosc Inactivation* in Fig. 9), which was calculated as the difference in the I_{Post}/I_{Pre} ratio with or without 100 μM (*R*)-roscovitine (see the legend to Fig. 9*A*). The analysis of variance revealed that the response of L-DI-containing chimeric channels to (*R*)-roscovitine was not significantly different from that of WT L-channels (LLLL) but was significantly different from response of NLLL, NLLN, and WT N-channels (NNNN). Together, these results demonstrate that L-DI is critical for the (*R*)-roscovitine enhancement of VDI.

As demonstrated in Fig. 4, the dose-response relationship for roscovitine-enhanced inactivation of WT L-channels shows positive cooperativity with a Hill coefficient of >2 (19), whereas WT N-channels respond to roscovitine with a Hill coefficient of 1 (14, 15). Our data support localization of the roscovitine binding site within L-DI, which predicts that LN*NN will show positive cooperativity in response to increasing (*R*)-roscovitine concentrations. This idea was tested by measuring the (*R*)-roscovitine dose response of the LN*NN chimera. As expected, the (*R*)-roscovitine-enhanced VDI of the LN*NN chimera (Fig. 7*A*) showed a steep dose-response relationship with the Hill coefficient of 2.3 (Fig. 7*C*). On the other hand, the NLLL chimera responded to (*R*)-roscovitine with a shallow dose-response relationship with the Hill coefficient of 0.6. The comparisons showed that the responses of LLLL and LN*NN to 100 μM (*R*)-roscovitine were significantly larger relative to either NLLL and NNNN (see also Fig. 9*A*, different data set). Thus, the LN*NN chimera responds to (*R*)-roscovitine like WT L-channels.

Interestingly, the converse is true for N-DI. The (*R*)-roscovitine-induced inhibition of WT N-channels results in roughly equal reduction of peak and end current during long (200- or 1000-ms) voltage steps (Fig. 5*B*). This effect is mimicked by NLLN (not shown) and NLLL (Fig. 7*B*) but not by LN*NN (Fig. 7*A*). We quantified this effect by measuring the difference in end current *versus* peak current inhibition (Δ *Inh End-Peak*) and compared that difference between the LLLL, LN*NN,

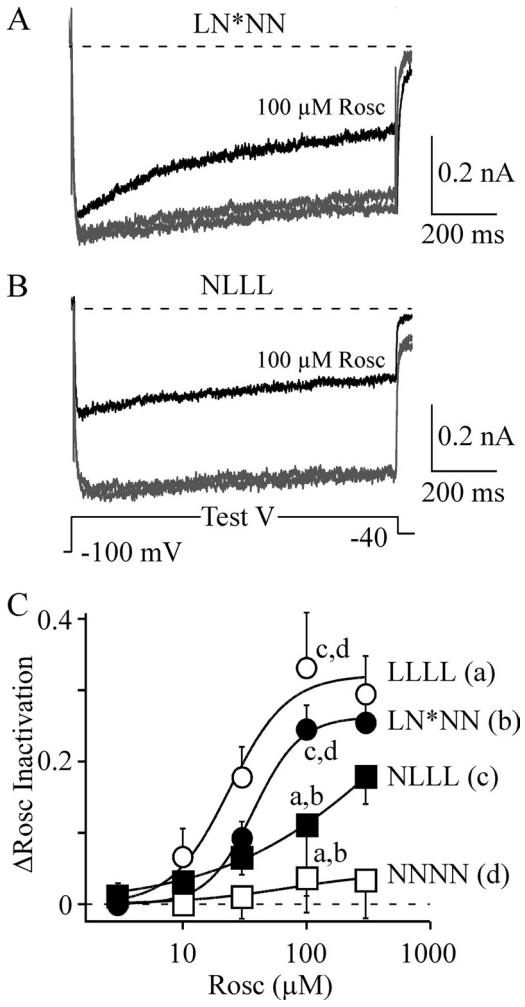

FIGURE 7. **Binding site properties for (*R*)-roscovitine-enhanced VDI follows L-DI.** *A*, the LN*NN chimera responds to 100 μM (*R*)-roscovitine (*Rosc, black trace*) with enhanced inactivation during 1-s steps to the voltage-generating maximal current (*Test V* = +30 mV). Note that the peak current early in the voltage step was little affected by roscovitine. *B*, the NLLL chimera responds to (*R*)-roscovitine (*black trace*) with a roughly equal inhibition of both peak and end current during 1-s steps to the voltage generating peak current (*Test V* = +10 mV). Note that inactivation during the voltage step was only weakly affected by (*R*)-roscovitine. *C*, the enhancement of inactivation induced by (*R*)-roscovitine was calculated as the difference in the I_{Post}/I_{Pre} ratio between control and Rosc (Δ*Rosc Inactivation*). This difference in inactivation is plotted *versus* (*R*)-roscovitine concentration for WT L-channels (LLLL) and WT N-channels (NNNN) as well as the LN*NN and NLLL chimeras. Inactivation was measured from 200-ms steps for LLLL and 1-s steps for the other three channel types. The *smooth lines* are fits using the Hill equation with EC_{50} = 24 μM and Hill coefficient = 1.9 for LLLL, EC_{50} = 37 μM and Hill coefficient = 2.3 for LN*NN, EC_{50} = 634 μM and Hill coefficient = 0.6 for NLLL, and EC_{50} = 72 μM and Hill coefficient = 1 (fixed) for NNNN. The *lowercase letters* indicate the data at 100 μM Rosc that differ significantly from LLLL (*a*), LN*NN (*b*), NLLL (*c*), and NNNN (*d*) (analysis of variance).

NLLL, NLLN, and NNNN channels (Fig. 9*C*). Consistent with our analysis of VDI, LLLL and LN*NN showed larger (*R*)-roscovitine-induced inhibition of end *versus* peak current, which resulted in a significantly larger Δ *Inh* value relative to NLLL, NLLN, or NNNN. The WT L-channel response to (*S*)-roscovitine was also statistically similar to that of (*R*)-roscovitine, which supports our conclusion that these drugs enhance VDI by binding to a common site (Fig. 4). On the other hand, the response to (*R*)-roscovitine of both N-DI-containing chimeras (NLLL and NLLN) was statistically similar to that of WT

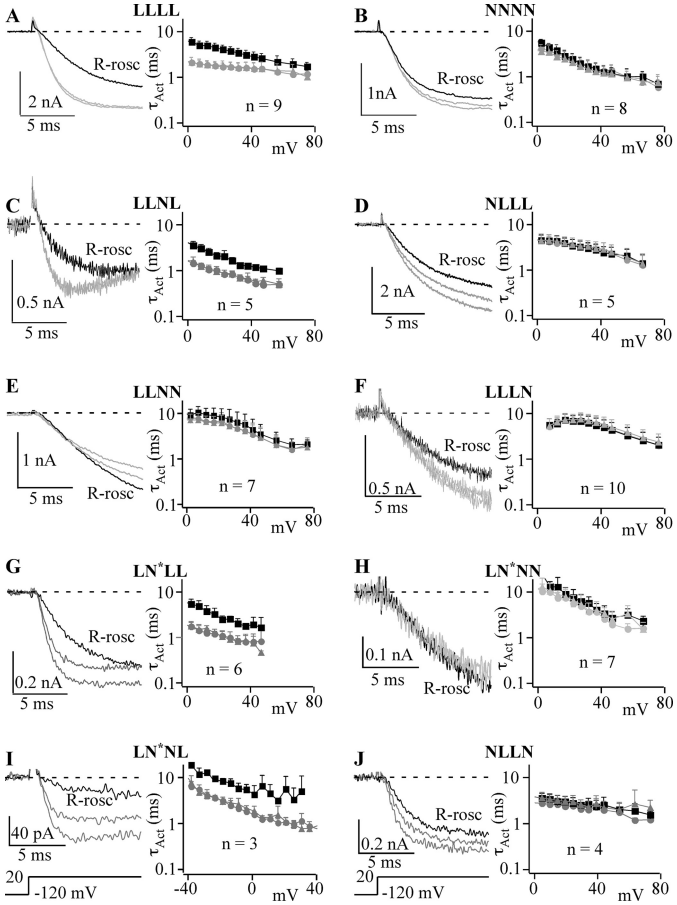

FIGURE 8. **(*R*)-Roscovitine-induced slowed activation requires L-DI and L-DIV.** Depending on the channel type, either 10 ms (NNNN (*B*) and LLNL (*C*)) or 25 ms (LLLL (*A*), LLNN (*E*), NLLL (*D*), LLLN (*F*), LN*LL (*G*), LN*NN (*H*), LN*NL (*I*), and NLLN (*J*)) voltage steps were used to determine the activation time constant (τ_{Act}) from single exponential fitting. In each *panel*, the *gray current traces* are control and washout, whereas the *black current traces* were recorded in the presence of 100 μM (*R*)-roscovitine (*R-rosc*). The *left portion* of each *panel* shows the τ_{Act} *versus* step voltage dependence with (*black symbols*) and without (*gray symbols*) 100 μM (*R*)-roscovitine averaged ± S.D. from the indicated number of cells. Control data are shown as *circles*, and recovery from roscovitine is shown as *triangles*. LLLL (*A*), LLNL (*C*), LN*LL (*G*), and LN*NL (*I*) chimeric channels showed slowed activation in the presence of (*R*)-roscovitine, whereas the activation of NNNN (*B*), NLLL (*D*), LLNN (*E*), LLLN (*F*), LN*NN (*H*), and NLLN (*J*) channels was not affected.

N-channels, but the response of all three channels was statistically different from that of either LN*NN or LLLL. Thus, the roscovitine binding site mediating N-channel inhibition appears to be localized to N-DI.

Slowed Activation—We investigated the effect of (*R*)-roscovitine on activation using short steps of either 10- or 25-ms duration (determined by activation kinetics) to voltages ranging from +10 to +70 mV (Fig. 8). Current traces elicited by voltage steps to +20 mV show the effect of 100 μM (*R*)-roscovitine on activation and that effect was further quantified by fitting activation using a single exponential equation to determine τ_{Act}, which was plotted *versus* step voltage to show the effect of (*R*)-roscovitine over a range of voltages. Using the approach that worked well for inactivation, we measured activation of the LLNN chimera, but (*R*)-roscovitine failed to slow activation (Figs. 8*E* and 9*B*). This suggests that L-DIII and/or L-DIV are important for the effect of (*R*)-roscovitine on activation. The critical domain appeared to be L-DIV, since (*R*)-roscovitine slowed activation of the LLNL chimera (Figs. 8*C* and 9*B*). The importance of L-DIV was further supported because activation of the LLLN chimera was not affected by (*R*)-roscovitine (Figs. 8*F* and 9*B*). Surprisingly, (*R*)-roscovitine also failed to affect activation of the NLLL chimera, which suggested that L-DI was also required for (*R*)-roscovitine-induced slowed activation. Consistent with this idea, LN*LL also responded to (*R*)-roscovitine with slowed activation, but LN*NN and NLLN did not (Figs. 8 and 9*B*). A critical test of our dual domain hypothesis was the LN*NL chimera, which responded to 100 μM (*R*)-roscovitine with slowed activation (Figs. 8*I* and 9*B*). Thus, both L-DI and L-DIV are both necessary and sufficient to mediate (*R*)-roscovitine-induced slowed activation.

DISCUSSION

Roscovitine, a promising drug with anticancer action (10, 22, 23), has recently been shown to affect voltage-dependent calcium channels (14–16, 19) and potassium channels (15, 24). From our previous findings (19), we generated the hypothesis that (*R*)-roscovitine-induced slowed activation and enhanced inactivation were mediated by a common binding site. However, this hypothesis was not supported by the present results. Our pharmacological data showed that the roscovitine receptor site mediating slowed activation (RR_{SA}) was stereo-selective, whereas the site mediating enhanced inactivation (RR_{EI}) was not. It appears that L-type channels contain two extracellularly exposed roscovitine binding sites. Our chimera data support localization of RR_{EI} to L-DI, whereas RR_{SA} appears to be composed of amino acids from both L-DI and L-DIV.

Pharmacological Separation of Roscovitine Effects on L-type Channels—We have previously shown that intracellularly applied (*R*)-roscovitine failed to affect L-channel kinetics and failed to abrogate the effects induced by externally applied (*R*)-roscovitine, which led us to conclude that (*R*)-roscovitine was interacting with an extracellularly exposed site to affect L-channel kinetics (19). Our results using (*S*)-roscovitine have enabled us to refine our original hypothesis to propose that there are two extracellularly exposed roscovitine binding sites. The stereo-selectivity of RR_{SA} permits enhanced inactivation to be examined in isolation by using (*S*)-roscovitine, which appears to exclusively activate the chiral-insensitive RR_{EI}. (*S*)-Roscovitine accelerated inactivation with the same potency as (*R*)-roscovitine, which shows that RR_{EI} is truly insensitive to the chiral carbon in the C2 side chain.

N-type channels also show two roscovitine-induced effects that are differentially affected by (*S*)-roscovitine (17, 18). The agonist effect of (*R*)-roscovitine (slowed deactivation) required at least a 20-fold higher (*S*)-roscovitine concentration, whereas the roscovitine-induced antagonist effect showed a similar IC_{50} for the two enantiomers (18). The two N-channel binding sites mediate effects that differ from those observed with L-channels. The N-channel agonist site appears to be revealed only upon channel activation (14, 15), whereas the antagonist site is linked to closed state (resting) inactivation (18). Thus, both types of voltage-dependent calcium channels (N-type and L-type) appear to have two roscovitine binding sites, one of

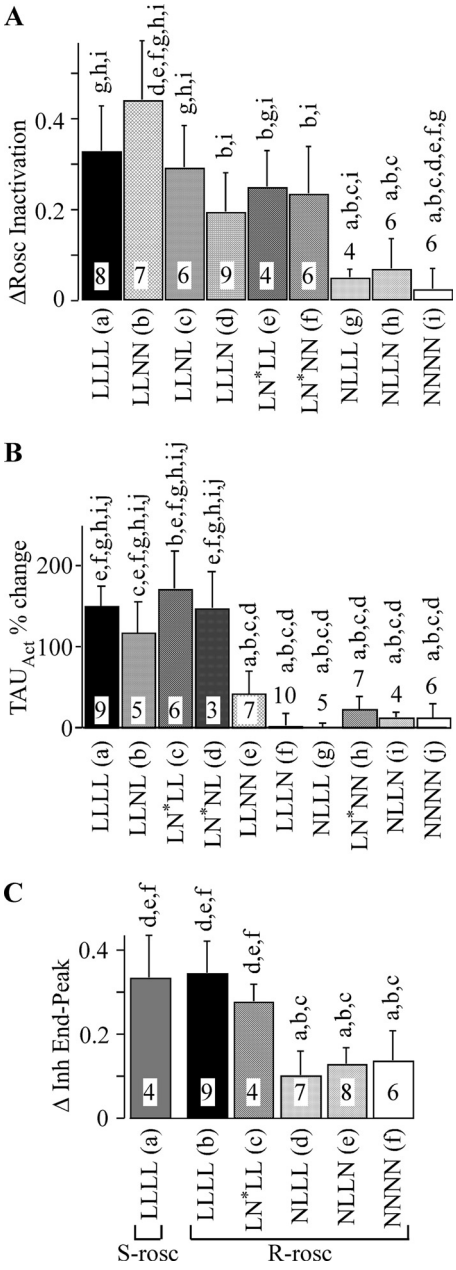

FIGURE 9. **(*R*)-Roscovitine-induced effects are mediated by different structures.** *A*, the enhancement of inactivation induced by 100 μM (*R*)-roscovitine was calculated as the difference in the I_{Post}/I_{Pre} ratio between control and (*R*)-roscovitine (Δ*Rosc Inactivation*). The inactivating step (200 ms) voltage used for this measurement was 20 mV for LLLL, 0 mV for LLNL, 30 mV for LLNN, 75 mV for LLLN, 30 mV for NLLL, 20 mV for LN*NN, 0 mV for LN*LL, 10 mV for NLLN, and 20 mV for NNNN. The significant differences were determined using analysis of variance with Tukey's HSD *post hoc* test ($p < 0.05$). The *lowercase letters above* each *column* indicate the data that differ significantly from LLLL (*a*), LLNL (*b*), LLNN (*c*), LLLN (*d*), LN*NN (*e*), LN*LL (*f*), NLLL (*g*), NLLN (*h*), and NNNN (*i*). The number of cells tested is listed *within* each *column*. *B*, (*R*)-roscovitine slows activation of channels composed of L-DI and L-DIV. The 100 μM (*R*)-roscovitine-induced percentage change in τ_{Act} measured during steps to 20 mV is shown for WT L- and N-channels as well as eight chimeras. The significant differences were determined using analysis of variance with Tukey's HSD *post hoc* test ($p < 0.05$). The *lowercase letters above* each *column* indicate the data that differ significantly from LLLL (*a*), LLNL (*b*), LN*LL (*c*), LN*NL (*d*), LLNN (*e*), LLLN (*f*), NLLL (*g*), LN*NN (*h*), NLLN (*i*), and NNNN (*j*). The number of cells tested is listed *within* each *column*. The control data for calculating the percentage change was the average of results obtained before and after recovery from (*R*)-roscovitine. *C*, the effect of roscovitine to inhibit peak *versus* end current was calculated as the difference of inhibition of peak current *versus* that at the end of the step (Δ *Inh End-Peak*). The effect of 100 μM (*R*)-roscovitine (*R-rosc*) was measured on LLLL, LN*NN, NLLL, NLLN, and NNNN, whereas that of 100 μM (*S*)-roscovitine (*S-rosc*) was measured on LLLL. Inhibition was measured from 200-ms steps for LLLL (20 mV) and 1000-ms steps for LN*NN (20 mV), NLLL (10 mV), NLLN (10 mV), and NNNN (20 mV). The number of cells tested is indicated. The *lowercase letters above* each *column* indicate the data that differ significantly from LLLL in (*S*)-roscovitine (*a*), LLLL in (*R*)-roscovitine (*b*), LN*NN (*c*), NLLL (*d*), NLLN (*e*), and NNNN (*f*). Note that there is no significant difference in the effect of (*S*)- *versus* (*R*)-roscovitine on LLLL.

which is stereo-selective. The stereo-specific sites affect the activation-deactivation process (slowed activation for L-channels and slowed deactivation for N-channels), whereas the stereo-insensitive sites are involved with inactivation (open state voltage-dependent inactivation for L-channels and closed state inactivation for N-channels).

Localization of the Roscovitine Binding Sites—With the apparent identification of multiple binding sites from the pharmacological experiments, we wanted to determine if these sites could be physically differentiated. Upon verification that the (*R*)-roscovitine-induced effects on N-type and L-type channels were unique, we utilized N-L chimeras to determine the domains containing the roscovitine binding sites. The chimeras were generated by "domain swapping" in an attempt to localize the binding sites using relatively few manipulations, and the technique was successful. However, a major problem was that chimeric channels containing N-DII failed to express measurable ionic currents, and sequencing showed that this did not result from unintended mutations in these chimeras. Our investigation demonstrated that the problem was within transmembrane segments S5 and S6 (the P-region) of N-DII, because L-channels containing just the N-DII P-region failed to generate measurable current, whereas current was reproducibly found in L-channels containing just the N-DII V-region (S1–S4). Thus, the engineered N-channel-like domain II (N*), which had transmembrane segments S1–S4 from N-channel and S5 and S6 from L-channel, allowed us to test the (*R*)-roscovitine effect on chimeric "N-channels" containing single L-channel domains.

The LLNN chimera was the first to be generated and demonstrated that RR_{EI} was localized to L-DI and/or L-DII, but the impaired slowed activation response of this chimera suggested that RR_{SA} could be within L-DIII or L-DIV. The strong (*R*)-roscovitine-induced slowed activation of the LLNL chimera along with the loss of that effect with the LLLN chimera supported L-DIV for RR_{SA}. However, the slowed activation effect was unexpectedly lost in the NLLL chimera, which along with the responsiveness of LLNL suggested that both L-DI and L-DIV were involved. This hypothesis was further supported by showing that (*R*)-roscovitine failed to alter activation of the NLLN chimera, whereas activation was slowed in the LN*LL chimera. The critical test was that (*R*)-roscovitine-induced slowed activation was transferred to the N-channel by inserting both L-DI and L-DIV to generate the LN*NL chimera. Thus, the evidence strongly supports the conclusion that RR_{SA} is formed by amino acid residues from both L-DI and L-DIV. It seems very likely that the site resides at the interface between L-DI and L-DIV, which suggests that (*R*)-roscovitine can be used as a probe to investigate structures within these domains that interact to form functional channels.

Although the RR_{SA} site appears to span two L-channel domains, we conclude that RR_{EI} is contained within L-DI. (*R*)-Roscovitine-enhanced VDI was observed in all chimeric channels containing L-DI, including LLNN, LLNL, LLLN, and LN*LL. The two critical tests of the L-DI hypothesis were the absence of enhanced inactivation of the NLLL chimera and the transfer of (*R*)-roscovitine-enhanced VDI to the N-channel by inserting L-DI to generate the LN*NN chimera. The dose-response for (*R*)-roscovitine-induced enhanced VDI was almost identical between LN*NN and WT L-channels, which strongly suggests that RR_{EI} is transferred to the N-channel by the insertion of L-DI. Thus, our results are consistent with the localization of RR_{EI} to L-DI and support the hypothesis that the two (*R*)-roscovitine-induced effects are mediated by physically distinct structures.

The Mechanism of Roscovitine-induced Inhibition—We previously concluded that both slowed activation and enhanced inactivation resulted from closed channel binding of (*R*)-roscovitine to a single site (19). This mechanism is still valid for (*R*)-roscovitine-induced slowed activation, but the discovery of a separate site for enhanced inactivation dictates a reevaluation of the mechanism for this effect. One clue comes from the dose-response relationship, where the Hill coefficient for the roscovitine-induced enhancement of inactivation is >2, which indicates positive cooperativity at RR_{EI}. A likely possibility is that the cooperativity results from transient binding site availability that would occur if (*R*)-roscovitine specifically interacted with the inactivated (VDI) state. The positive cooperativity occurs because at low roscovitine concentrations, the on-rate is much lower than the mean dwell time of the channel in the inactivated state, so the effective binding is small relative to a site that is constantly available. As the concentration increases, the effective on-rate becomes high enough for roscovitine to bind during the brief sojourns into the inactivated state.

One problem with this putative mechanism is that roscovitine can still enhance inactivation of L-D1-containing channels that show little or no inactivation under control conditions (*e.g.* LLLN and LN*LL). This phenomenon has also been observed in L-channel containing the Timothy syndrome mutation that abrogates VDI, but roscovitine can still enhance inactivation (40). This suggests that the development of the inactivated state is not required to reveal RR_{EI}. A likely alternative hypothesis is that a voltage-dependent conformational change in L-DI is required for roscovitine binding. One scenario is that the outward movement of L-DI S4 is the trigger that reveals RR_{EI}. Further work is required to more precisely determine the mechanism for roscovitine-enhanced VDI, but the available evidence suggests that roscovitine binding moves the inactivation gate, and it is not the movement of the inactivation gate that permits roscovitine binding.

Our hypothesis of L-DI containing RR_{EI} fits with the current idea that the L-channel I-II linker and domain IS6 form part of a "hinged lid" that mediates VDI (27). It seems that roscovitine binding to RR_{EI} in L-DI induces a conformational change that speeds movement of the hinged lid so that VDI becomes faster. In addition, this conformational shift may impede the reopening of the inactivation gate, which would explain the slowed recovery from inactivation that we observed previously (19).

Unique Binding Sites for 2,6,9-Trisubstituted Purine Antagonists—Calcium channel antagonists play an important role in treatment of neurological and cardiovascular diseases (6). L-type channel antagonists, such as dihydropyridines, phenylalkylamines, and benzothiazepines, are used for treatment of hypertension and angina pectoris (4, 5, 7, 8, 28, 29). The dihydropyridine, phenylalkylamine, and benzothiazepine binding sites appear to encompass separate but partially overlapping regions located within domains III and IV (30–32). The effect of (*R*)-roscovitine on the LLNN chimera demonstrates that RR_{EI} is a unique binding site on L-type calcium channels. Therefore, roscovitine (*R* and S) represents a new class of L-channel antagonists that induce L-channel inhibition by enhancing VDI without affecting closed state inactivation (19).

Activation of RR_{SA} is unique among calcium channel antagonists, and such drugs could have an important clinical use in preventing reactivation of L-type channels that generate proarrhythmic events, such as early afterdepolarizations (33–36). In addition, activation of RR_{EI} could have important therapeutic effects for cardiac arrhythmias resulting from this "rebound" L-channel activity on the falling phase of the cardiac afterdepolarization (*e.g.* Torsades de Pointes) (35–37). Recordings of L-current stimulated by a cardiac afterdepolarization waveform show that (*R*)-roscovitine preferentially inhibits current late in the afterdepolarization as expected from enhanced VDI (19). In addition, activation of RR_{EI} could normalize L-channel activity in patients suffering from genetic disorders that slow VDI, such as Timothy syndrome (38–40). Indeed, we recently demonstrated that (*R*)-roscovitine could normalize inactivation of L-channels carrying the Timothy syndrome mutation (40). The further characterization of both RR_{SA} and RR_{EI} could lead to the development of a new class of drugs that specifically target L-type channels to control arrhythmic behavior by slowing activation and enhancing VDI.

Acknowledgment—We thank Yunhua Wang for technical assistance.

REFERENCES

1. Striessnig, J., Hoda, J. C., Koschak, A., Zaghetto, F., Müllner, C., Sinnegger-Brauns, M. J., Wild, C., Watschinger, K., Trockenbacher, A., and Pelster, G. (2004) *Biochem. Biophys. Res. Commun.* **322,** 1341–1346
2. Bourinet, E., Mangoni, M. E., and Nargeot, J. (2004) *J. Clin. Investig.* **113,** 1382–1384
3. Roden, D. M., Balser, J. R., George, A. L., Jr., and Anderson, M. E. (2002) *Annu. Rev. Physiol.* **64,** 431–475
4. Glasser, S. P., Neutel, J. M., Gana, T. J., and Albert, K. S. (2003) *Am. J. Hypertens.* **16,** 51–58
5. Bai, R. (2005) *Clin. Cardiol.* **28,** 343–348
6. Elmslie, K. S. (2004) *J. Neurosci. Res.* **75,** 733–741
7. Suzuki, S., Ohtsuka, S., Ishikawa, K., and Yamaguchi, I. (2003) *Hypertens. Res.* **26,** 193–199
8. Thomas, M. G., Sander, G. E., Given, M. B., Quiroz, A. C., Roffidal, L. E., and Giles, T. D. (1990) *J. Clin. Pharmacol.* **30,** 24–28
9. Meijer, L., and Raymond, E. (2003) *Acc. Chem. Res.* **36,** 417–425
10. Benson, C., White, J., De Bono, J., O'Donnell, A., Raynaud, F., Cruickshank, C., McGrath, H., Walton, M., Workman, P., Kaye, S., Cassidy, J., Gianella-Borradori, A., Judson, I., and Twelves, C. (2007) *Br. J. Cancer* **96,** 29–37
11. Vitali, L., Yakisich, J. S., Vita, M. F., Fernandez, A., Settembrini, L., Siden, A., Cruz, M., Carminatti, H., Casas, O., and Idoyaga Vargas, V. (2002)

Cancer Lett. **180,** 7–12
12. Raynaud, F. I., Whittaker, S. R., Fischer, P. M., McClue, S., Walton, M. I., Barrie, S. E., Garrett, M. D., Rogers, P., Clarke, S. J., Kelland, L. R., Valenti, M., Brunton, L., Eccles, S., Lane, D. P., and Workman, P. (2005) *Clin. Cancer Res.* **11,** 4875–4887
13. McClue, S. J., Blake, D., Clarke, R., Cowan, A., Cummings, L., Fischer, P. M., MacKenzie, M., Melville, J., Stewart, K., Wang, S., Zhelev, N., Zheleva, D., and Lane, D. P. (2002) *Int. J. Cancer* **102,** 463–468
14. Buraei, Z., Anghelescu, M., and Elmslie, K. S. (2005) *Biophys. J.* **89,** 1681–1691
15. Buraei, Z., Schofield, G., and Elmslie, K. S. (2007) *Neuropharmacology* **52,** 883–894
16. Yan, Z., Chi, P., Bibb, J. A., Ryan, T. A., and Greengard, P. (2002) *J. Physiol.* **540,** 761–770
17. Cho, S., and Meriney, S. D. (2006) *Eur. J. Neurosci.* **23,** 3200–3208
18. Buraei, Z., and Elmslie, K. S. (2008) *J. Neurochem.* **105,** 1450–1461
19. Yarotskyy, V., and Elmslie, K. S. (2007) *Br. J. Pharmacol.* **152,** 386–395
20. Grabner, M., Wang, Z., Hering, S., Striessnig, J., and Glossmann, H. (1996) *Neuron* **16,** 207–218
21. Goo, Y. S., Lim, W., and Elmslie, K. S. (2006) *J. Neurophysiol.* **96,** 1075–1083
22. Meijer, L. (1996) *Trends Cell Biol.* **6,** 393–397
23. Wesierska-Gadek, J., Schmitz, M. L., and Ranftler, C. (2007) *J. Cell. Biochem.* **100,** 865–874
24. Ganapathi, S. B., Kester, M., and Elmslie, K. S. (2009) *Am. J. Physiol.* **296,** C701–C710
25. Peterson, B. Z., DeMaria, C. D., Adelman, J. P., and Yue, D. T. (1999) *Neuron* **22,** 549–558
26. Peterson, B. Z., Lee, J. S., Mulle, J. G., Wang, Y., de Leon, M., and Yue, D. T. (2000) *Biophys. J.* **78,** 1906–1920
27. Stotz, S. C., Jarvis, S. E., and Zamponi, G. W. (2004) *J. Physiol.* **554,** 263–273
28. Pellinen, T. J., Lukkala, K., Sundberg, S., Heikkilä, J., and Frick, M. H. (1992) *Ann. Med.* **24,** 49–53
29. Pepine, C. J., Handberg, E. M., Cooper-DeHoff, R. M., Marks, R. G., Kowey, P., Messerli, F. H., Mancia, G., Cangiano, J. L., Garcia-Barreto, D., Keltai, M., Erdine, S., Bristol, H. A., Kolb, H. R., Bakris, G. L., Cohen, J. D., and Parmley, W. W. (2003) *JAMA* **290,** 2805–2816
30. Striessnig, J., Grabner, M., Mitterdorfer, J., Hering, S., Sinnegger, M. J., and Glossmann, H. (1998) *Trends Pharmacol. Sci.* **19,** 108–115
31. Striessnig, J. (1999) *Cell Physiol. Biochem.* **9,** 242–269
32. Hockerman, G. H., Peterson, B. Z., Johnson, B. D., and Catterall, W. A. (1997) *Annu. Rev. Pharmacol. Toxicol.* **37,** 361–396
33. Carmeliet, E. (1999) *Physiol. Rev.* **79,** 917–1017
34. Bers, D. M. (2002) *Circ. Res.* **90,** 14–17
35. Ter Keurs, H. E., and Boyden, P. A. (2007) *Physiol. Rev.* **87,** 457–506
36. Thomas, G., Gurung, I. S., Killeen, M. J., Hakim, P., Goddard, C. A., Mahaut-Smith, M. P., Colledge, W. H., Grace, A. A., and Huang, C. L. (2007) *J. Physiol.* **578,** 85–97
37. Nerbonne, J. M., and Kass, R. S. (2005) *Physiol. Rev.* **85,** 1205–1253
38. Splawski, I., Timothy, K. W., Sharpe, L. M., Decher, N., Kumar, P., Bloise, R., Napolitano, C., Schwartz, P. J., Joseph, R. M., Condouris, K., Tager-Flusberg, H., Priori, S. G., Sanguinetti, M. C., and Keating, M. T. (2004) *Cell* **119,** 19–31
39. Splawski, I., Timothy, K. W., Decher, N., Kumar, P., Sachse, F. B., Beggs, A. H., Sanguinetti, M. C., and Keating, M. T. (2005) *Proc. Natl. Acad. Sci. U.S.A.* **102,** 8089–8096; discussion 8086–8088
40. Yarotskyy, V., Gao, G., Peterson, B. Z., and Elmslie, K. S. (2009) *J. Physiol.* **587,** 551–565